Support Information Material

A High-sensitivity electrochemical sensor based on double template molecularly imprinted polymer for simultaneous determination of Clenbuterol hydrochloride and Ractopamine

Xiang Li [a], Yangguang Li [a], Pai Yu [a], Yanbin Tong [a], Bang-Ce Ye [a, b*]

[a] Key Laboratory for Green Processing of Chemical Engineering of Xinjiang Bingtuan, School of Chemistry and Chemical Engineering, Shihezi University, Shihezi, China.

[b] Institute of Engineering Biology and Health, Collaborative Innovation Center of Yangtze River Delta Region Green Pharmaceuticals, College of Pharmaceutical Sciences, Zhejiang University of Technology, Hangzhou 310014, Zhejiang,China,

*Corresponding authors: Bang-Ce Ye. Tel/Fax: +86-021-64252094. E-mail address: bcye@ecust.edu.cn

1. Instruments and reagents

N, N-dimethylformamide (DMF), ethanol, $FeCl_3 \cdot 6H_2O$ hexahydrate, terephthalic acid, and 2-Aminoterephthalic acid were all purchased from Adamas Regent Co. Ltd (Shanghai, China). Reagents and materials, such as $FeCl_3 \cdot 6H_2O$, NaOH, H_2SO_4, methanol, clenbuterol, and ractopamine, are all analytically pure. All the solutions were prepared by distilled water and ultrasonically treated with SY-360 Ultrasonic Cleaner Co. Ltd.

The electrochemical measurement was carried out on the electrochemical workstation of Chi 760e. The traditional three-electrode system includes a bare or modified planar glass carbon electrode (GCE) diameter of 4 mm as the working electrode, saturated mercury electrode (SCE) as the reference electrode, and a platinum wire (0.5 mm in diameter and 34 mm in length) as the paired electrode. The morphology of the material was characterized by the 10 kV blue Xflash-SDD-5010 scanning electron microscope (SEM) from Germany. The surface area of the polymer was measured using a quantachrome Nova 1000 based on the Bruneau–Emmett–Teller experiment, and the X-ray diffraction (XRD) patterns of all samples were analyzed by a RIGAKU Giegerflex D/max B diffractometer with Cu-Kα radiation. The scanning steps and speeds were 0.02° and 0.01°/min, respectively, and the samples were scanned in the range of 10°-80° angle. Surface composition and chemical state wereperformed with X-ray photoelectron spectroscopy (XPS) equipped with an MGK α X-ray source (1253.6 eV), Thermo ESCALab 250 xi from Thermo Fisher Scientific, Waltham, Ma, USA, under a vacuum pressure of less than 10^{-6} Pa. The MOF material was pretreated with a centrifuge.

2. Optimization of preparation conditions of materials and electrodes

2.1 Optimization of Calcination temperature

When N@Fe-MOF was calcined at high temperatures, the calcination temperature was optimized, as shown in Fig. S1A. When the calcination temperature was 700 ℃, the cyclic voltammetry (CV) current response of N@Fe-MOF@C was found to be the largest. It is thus concluded that 700 ℃ is the best calcination temperature.

2.2 Optimal diagram of ligand regulation

The figure of ligand regulation optimization can be seen in the Fig. S1B.

2.3 Optimization of dropping amount

The dropping amount of N@Fe-MOF@C on bare glass carbon electrode was optimized. The results are shown in Fig. S1C. When the dropping amount is 10 μL, the CV current response of the prepared N@Fe-MOF@C/GCE is the largest, thus 10 μL is the best material dropping amount.

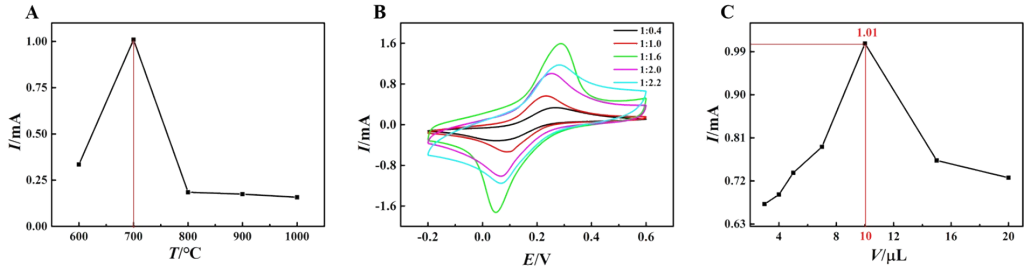

Figure S1. Optimization of N@Fe-MOF@C carbonization temperature(A); Cyclic voltammetric scanning of different ligand ratios of N@Fe-MOF(B); Dropping amount optimization of N@Fe-MOF@C(C).

3. Study on the adsorption of CLB and RACD by N@Fe-MOF@C

In order to study the adsorption effect of N@Fe-MOF@C itself on CLB and RAC, a series

of adsorption experiments were carried out. Using UV spectrophotometry as the standard method, the adsorption standard curves of N@Fe-MOF@C for CLB and RAC were established. After calculation, two standard curves were obtained: A_{CLB}= 7735c−0.0925, R^2 = 0.9999; A_{RAC}= 1765.8c−0.0607, R^2 = 0.9991. As shown in the static adsorption isotherm in Fig. S2-1A, the binding capacity of N@Fe-MOF@C to CLB gradually increased in the CLB solution from 0.04 mM to 0.1mM, but when its concentration was 0.1mM, the increasing rate of binding capacity obviously slowed down and gradually approached a constant value. The results showed that N@Fe-MOF@C was saturated with CLB and reached adsorption equilibrium, and the maximum binding capacity was 6.81mg g^{-1}. It can also be seen from Fig. S2-1B that the adsorption capacity of N@Fe-MOF @C gradually increases in the RAC solution of 0.1mM to 0.6mM, and when the adsorption capacity exceeds 0.6mM, the adsorption capacity gradually tends to a constant value, that is, the adsorption equilibrium is reached, and the maximum adsorption capacity is 9.97mg g^{-1}.

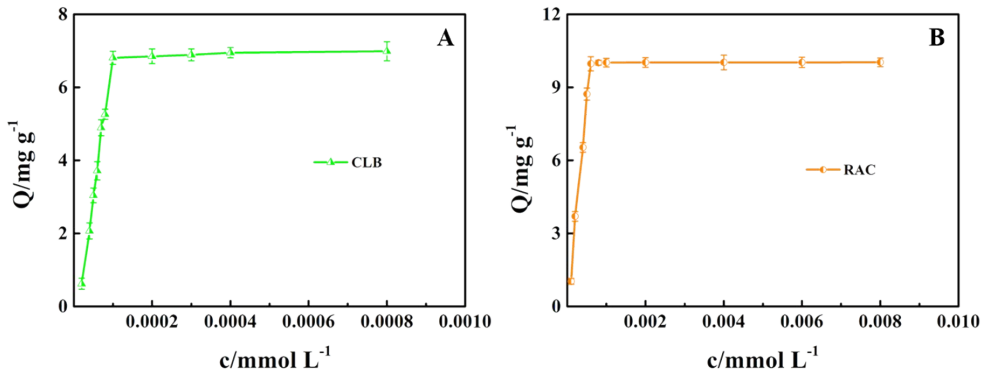

Figure S2-1. N@Fe-MOF@C Static adsorption curves of CLB and RAC. Error bars represent means ± the variation range of triplicates.

Fig. S2-2 illustrates the adsorption behavior of N@Fe-MOF@C on CLB and RAC over time. The adsorption capacity of N@Fe-MOF@C for CLB increased at first and then tended to

balance. When the adsorption time was 120min, the adsorption capacity of N@Fe-MOF@C for CLB was 3.16mg g^{-1}, which basically reached the adsorption equilibrium. The binding amount of N@Fe-MOF@C to RAC was consistent with the trend of CLB, and its maximum adsorption capacity was 1.0017mg g^{-1}. The above studies showed that N@Fe-MOF@C also had certain adsorption effects on CLB and RAC. The binding phenomenon showed that the complex cluster network of N@Fe-MOF@C had a large number of tiny hole structures, so it could bind CLB and RAC rapidly. As the outer surface binding gradually reached equilibrium, CLB and RAC began to transfer mass to the deep hole, and there would be a certain steric hindrance effect at this time, leading to a significant decrease in the binding rate until equilibrium.

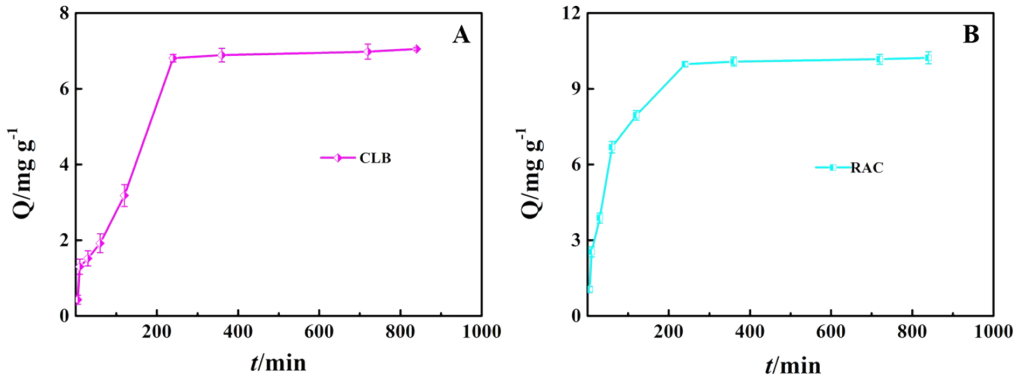

Figure S2-2. N@Fe-MOF@C Dynamic adsorption curves of CLB(A) and RAC(B). Error bars represent means ± the variation range of triplicates.

4. Characterization by atomic force microscopy

The surface morphology and roughness of the molecular imprinting process were characterized by atomic force microscopy (AFM). As can be seen from Fig. S3A, the surface of the molecularly imprinted glassy carbon electrode is relatively rough, with a roughness of Rq=61.8 nm. And as shown in Fig. S3B, the surface of the glassy carbon electrode modified by

non-imprinted polymer is smoother and the roughness is Rq=36.0nm. The loose surface morphology is beneficial to the recognition of template molecules by imprinted polymer.

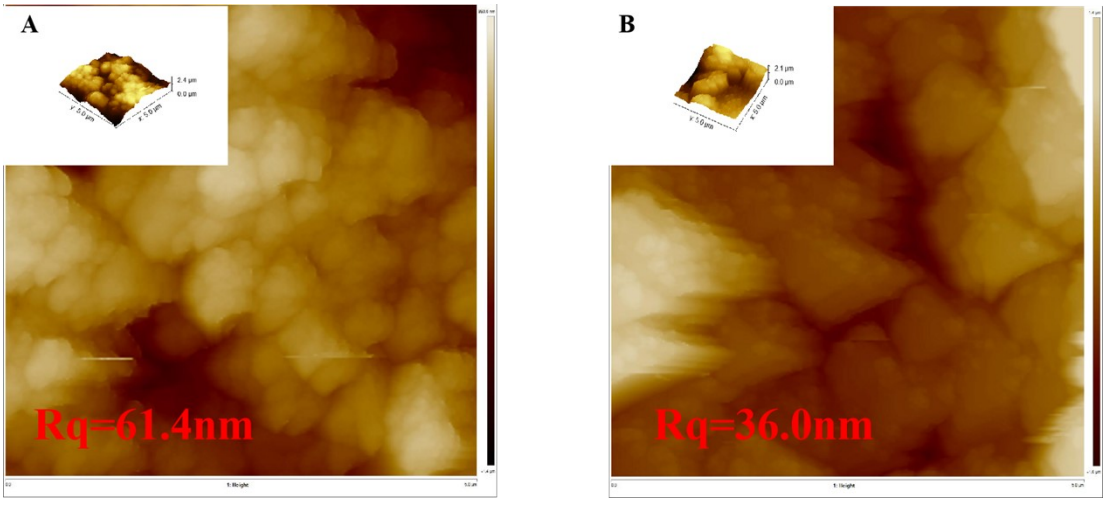

Figure S3. Atomic force microscopy (AFM) images of molecularly imprinted polymers(A) and non-imprinted polymers(B).

5. Table of DTMIP adsorption of CLB and RAC

Table S1. Competitive loading of CLB, RAC and DA by the DTMIP and NIP.

Sorbent	Capacity (mg g^{-1})			K_D (mL g^{-1})			α		β	
	CLB	RAC	DA	CLB	RAC	DA	CLB/DA	RAC/DA	CLB/DA	RAC/DA
DTMIP	19.75	18.99	1.24	0.21	0.19	0.02	10.50	9.50	8.75	7.92
NIP	15.23	13.52	12.98	0.06	0.06	0.05	1.20	1.20		

6. Actual sample detection

Table S2. Using N@Fe-MOF@C/DTMIP/GCE (N=3) to determine CLB and RAC in real samples.

Sample	Detectable substance	Determined(μM)	Spiked(μM)	Total found(μM)	Recovery (%)	RSD (%)
Urine sample	CLB	4.27×10^{-6}	10^{-5}	1.432×10^{-5}	100.5	1.06
		4.27×10^{-6}	2.0×10^{-5}	2.382×10^{-5}	97.8	2.83

		4.27×10^{-6}	3.0×10^{-5}	3.391×10^{-5}	98.8	1.97
		—	10^{-5}	0.974×10^{-5}	97.4	2.10
	RAC	—	2.0×10^{-5}	2.052×10^{-5}	102.6	3.01
		—	3.0×10^{-5}	3.037×10^{-5}	101.2	2.23
		3.94×10^{-6}	10^{-5}CLB,10^{-5}RAC	2.389×10^{-5}	99.8	2.12
Raw pork	CLB, RAC	3.94×10^{-6}	2×10^{-5}CLB,2×10^{-5}RAC	4.421×10^{-5}	100.7	2.21
		3.94×10^{-6}	3×10^{-5}CLB,3×10^{-5}RAC	6.408×10^{-5}	100.2	3.17

97